Conductivity, Diffusivity and Free Charge Density in Mixed Salts Based on CsH_2PO_4 Under Humid Atmosphere Conditions

Andreu Andrio[a], S. I. Hernández[b], C. García-Alcántara[b], Iván Santamaría-Holek[b], L. F. del Castillo[c], Vicente Compañ[d,*]

[a]Departamento de Física. Universitat Jaume I.12080-Castellón (Spain), E-mail: andrio@uji.es
[b]Unidad Multidisciplinaria de Docencia e Investigación-Juriquilla, Facultad de Ciencias, Universidad Nacional Autónoma de México (UNAM), Juriquilla, Querétaro, CP 76230, Mexico, E-mail: saul.ivan.hernandez@unam.mx ; consuelo.garcia@unam.mx ; isholek.fc@gmail.com
[c]Departamento de polímeros, Instituto de Investigaciones en Materiales, Universidad Nacional Autónoma de México (UNAM), Ciudad Universitaria, Apartado Postal 70-360, Coyoacán, Ciudad de México, 04510, México. E-mail: lfelipe@unam.mx
[d]Departamento de Termodinámica Aplicada. Universidad Politécnica de Valencia. C/Camino de Vera s/n, 46022-Valencia (Spain).

(*) Author corresponding: Email: vicommo@ter.upv.es

ABSTRACT

Impedance spectroscopy measurements at different temperatures in humid conditions were performed in different mixed acid salts based on phosphates of CsH_2PO_4. In these compounds a superprotonic phase transition is observed, accompanied by a morphological phase transition with the increase on the temperature, (monoclinic (low temperature) to cubic phase (high temperature)). In this work, the influence of the Ba, Rb, W, Mo and S on the conductivity, diffusivity and free charge density of the compounds is studied. The partial substitution of Cs by Rb shows the highest conductivity, and in the case of Ba and S the conductivity is significant at low temperatures. The conductivity, the diffusivity of the protons, the free protonic charge density, and the static permittivity were calculated using the electrode polarization (EP) model, considering a Cole-Cole function for the permittivity. It is observed a growth in conductivity when the high-temperature phase is reached for most samples. When the phase changes a decrease in the activation energy takes place, in agreement with an order-disorder protonic transition type. This study provides with a new paradigm to design heterogeneous solid electrolytes to be used in electrochemical devices, including fuel cells and supercapacitors.

1. INTRODUCTION

Nowadays, the common used solid electrolytes are based on polymers such as Nafion®, which are limited to be handle at low temperatures (below 100ºC),[1] and mixed electronic ionic oxides which operate at high temperatures (above 500-600ºC).[2] On the other hand, pyrophosphates of tetravalent metals (MP_2O_7, M=Sn, Zr, Ce, Ti, etc.) and its compounds, have been potential candidates to be applied as solid electrolytes for intermediate temperature (in the range of 220ºC to 250ºC) proton exchange membrane fuel cells,[3] but they have a poor sintering ability at these temperatures.

The use of heterogeneous composites as solid electrolytes on fuel cells, electrolytes and supercapacitors, constitutes a field to explore new materials, whose electrochemical properties must be known. For instance, the acidic salts of cesium dihydrogen phosphate CsH_2PO_4 (CsP) show a phase transition from a low-temperature monoclinic phase to a

high-temperature cubic phase at high contents of water (above 30 %). In the cubic phase (above 210ºC), the conductivity has a higher value than in the monoclinic phase (below 200ºC).[4,5] This is described as a superprotonic phase transition leading to an abrupt increase in the conductivity, and it occurs reversibly above 200ºC in humid conditions. It is also observed in CsP/silica compounds,[6] but it is notable that this has not been seen under dry conditions in compounds such as MH_2PO_4 (M= K, Rb, Cs),[7,8] which are good protonic conductors. This fact is associated to chemical reaction like dehydration by one side,[8] and to a structural phase transition by another.[9]

So, it is important to get information about the influence of the material properties on the high-performance ion-conduction, through the knowledge of the value of the conductivity as a function of temperature, and the mechanism of the diffusivity of protons or ions into the systems.[10,11] In this way, several approaches have been developed to determine the ion diffusivity and the free-charge density under impedance spectroscopy analysis.[12-24] Some of these approaches involve the macroscopic polarization of mobile charges, which is influenced by changes of crystallinity and other electrode effects.[10,13-16,19]

In this work, the partial substitution of Cs by Rb and Ba, to give Cs_{1-x} $Rb_xH_2PO_4$ and Cs_{1-x} $Ba_{0.5x}H_2PO_4$, named (CsP-Rb) and (CsP-Ba) respectively, were synthesized in order to study the proton conductivity, diffusivity and charge carriers density. On the other hand, also were studied a series of metal phosphates compounds produced by mixing the solutions formed by CsH_2PO_4 with others compounds containing Tungsten (CsP-W) and Molybdenum (CsP-Mo), as well as the compound named (CsP-S) prepared from mixed the aqueous solution of initial components CsH_2PO_4 and $CsHSO_4$. Our purpose is to analyze the effect of temperature, and the effect of different dopants/substituents (S, Ba, W, Rb and Mo) on the conductivity, diffusivity and free charge density respect to the acidic salt of cesium dihydrogen phosphate CsH_2PO_4 (CsP) in humid conditions. An EP model introduced by Klein *et al.*[10] is followed to determine the free-charge density and diffusion coefficient, from the analysis of the frequency dependence of complex dielectric loss ε" and loss tan δ. Since the EP analysis overestimate the free proton diffusivity while underestimate the free proton number density providing lower values for the free-charge density than the total number of ionic species available from the preparation of the compounds, and then overestimating the proton diffusivity, we follow the same line of reasoning that Wang *et al.*[23], who have corrected both the number density and the diffusion coefficient. On the other hand, for comparison, an analysis is made on protons diffusivity values in the solid electrolytes considering also the Macdonald-Trukhan model.[11,13,15,16,22-24] The Eyring rate processes theory and the Arrhenius behavior on the conductivity are used to find the activation thermodynamic parameters. Finally, the test of the Serghei formula is introduced[20] to calculate the real part of the permittivity, in order to make a comparison with the estimated value from Klein *et al.*[10] model.

2. EXPERIMENTAL SECTION

2.1 Samples preparation

The powder of CsH_2PO_4 (CsP) was prepared from aqueous solutions of Cs_2CO_3 and H_3PO_4 in a molar ratio of 1:2.[25] From CsH_2PO_4 different orthophosphates, based on the partial substitution of Cs by Rb and Ba, to give Cs_{1-x} $Rb_xH_2PO_4$ and Cs_{1-x} $Ba_{0.5x}H_2PO_4$, named (CsP-Rb) and (CsP-Ba) respectively, were synthesized. The mixed samples of CsH_2PO_4/ RbH_2PO_4 (CsP-Rb) and CsH_2PO_4/$Ba(H_2PO_4)_2$ (CsP-Ba) at 80:20 w/w were

prepared using the adequate concentrations of Rb_2CO_3 and $BaCO_3$, respectively. A viscous paste was obtained and further heat treated at temperatures ranging from 300 to 800ºC to calcinate. The obtained phosphates were then ground to powder.
On the other hand, the compound named (CsP-S) were prepared from aqueous solution of initial components CsH_2PO_4 and $CsHSO_4$ with adequate concentrations to get a mixed polycrystalline of 80:20 w/w. Finally, to obtain the powders of composites named (CsP-Mo) and (CsP-W), we have mixed the solutions formed by CsH_2PO_4 with $H_3Mo_{12}PO_{40}{\cdot}xH_2O$ to get the polycrystalline sample (CsP-Mo), and with $H_3W_{12}PO_{40}{\cdot}xH_2O$ to obtain the mixture of cesium phosphate with Keggin salt of tungsten (CsP-W). In both cases, we have employed adequate concentrations to get a 80:20 w/w. Precipitation was promoted adding ethanol. A viscous paste was obtained and further heat treated at 150ºC to obtain the powders of mixed samples named (CsP-S), (CsP-Mo) and (CsP-W), respectively. Disk samples were used for impedance electrochemical measurements with a diameter of 13 mm and thickness of 1.6 mm, being produced by uniaxial pressing.

2.2. Samples composition and morphology

The morphology of the samples CsP, CsP-Ba, CsP-Rb, CsP-S and CsP-Mo was examined using a scanning electron microscope (SEM) Quanta 200 FEG-ESEM (FEI Company) coupled to an Energy Dispersive X-Ray spectrometer (EDX) for elemental analysis of Cs, P and Ba, Rb, S, W and Mo, operating at an acceleration voltage of 15 kV, pressure at 60 Pa and low vacuum. Samples were prepared by depositing few mg of powder sample on top of a carbon support. In supplementary information we can see, (Figures S1 to S5), the SEM images and EDX analysis of the sample CsP, CsP-Ba, CsP-Rb, CsP-S and CsP-Mo, respectively. With the atomic % of Cs and P and Ba, Rb, S, W and Mo we can compute the chemical composition of every sample. For the case of CsP the atomic ratio between Cs and P is 1/1.02 that matches accurately to the chemical formula CsH_2PO_4.

For CsP-Ba the atomic ratios Cs/P and Ba/P are 0.66 and 0.36, respectively that corresponds to a mix of CsH_2PO_4. 0,5 $BaHPO_4$. A similar situation is encountered for CsP-Rb where ratios Cs/P and Rb/P are 1.07 and 0.28, (see figure SI3) giving a formula $0.8Rb(H_2PO_4).(Cs_2(HPO_4).(Cs(H_2PO_4)$.

For CsP-S the atomic ratios according to EDX, (see figure SI4), on Cs/P= 51 and Cs/S= 1.85 of the mixtures of Cs_2SO_4 and CsH_2PO_4 with the addition of H_2SO_4 immediately suggest that the mixture will be basically made of Cs_2SO_4 with some impurity due to CsH_2PO_4. The best fit corresponds to 0.96 Cs_2SO_4. $0.04CsH_2PO_4$.

Similarly the mixing of $H_3Mo_{12}PO_{40}{\cdot}xH_2O$ and CsH_2PO_4, sample CsP-Mo, produces according to the EDX, (see figure SI5), a Mo/P and Cs/P ratios of 0,25 and 2.45, respectively that, as for CsP-S suggests that one of the components, in this case $H_3Mo_{12}PO_{40}{\cdot}xH_2O$ can be considered as an impurity. The overall formula is $3(Cs_2HPO_4).2(Cs_3PO_4)$.

2.2 Impedance measurements

Impedance measurements were carried out on polycrystalline samples at several temperatures lying in the range 423 K (150ºC) to 513 K (250ºC), and frequency window $10^{-1} < f < 10^7$ Hz. The experiments were performed with 100 mV amplitude, using a

Novocontrol broadband dielectric spectrometer (Hundsangen, Germany) integrated by a SR 830 lock-in amplifier with an Alpha dielectric interface. In previous measurements, different voltages (0.1, 0.5 and 1V) were considered with the intention to ensure the linear response. From the results observed we have considered that 100 mV is the appropriate in order to get a linear regime. For that purpose, electrodes made of graphite sheets were attached to both sides of the polycrystalline sample by co-pressing the synthesized materials in a sandwich cell configuration. The measurements were made following two different procedures.

1) Dry procedure: The powder of interest was sandwiched between two graphite sheets and introduced between two gold circular electrodes coupled to the impedance spectrometer. The assembly membrane-electrode was annealed in the Novocontrol setup under an inert dry nitrogen atmosphere, previously to the start of the actual measurement. For this experiment, the temperature was two times gradually raised and lowered from 150ºC to 250ºC in steps of 10ºC. At the third cycle of the temperature scan, the dielectric spectra were collected in each step. This procedure was performed to ensure the measurements reproducibility.

2) Wet procedure: The sandwiched sample of interest was wired by two porous stainless steel circular electrodes, were set in a glass tube, and then Nitrogen or 30% N_2/H_2O gaseous mixture was flowed through the tube at atmospheric pressure. In the same way as has been done in dry conditions, the temperature was two times gradually raised and lowered from 150ºC to 250ºC in steps of 10ºC. Also to ensure the measurements reproducibility, the values considered in our study were obtained from the third cycle of temperature scan. During the conductivity measurements, the temperature was kept constant or changed stepwise in all the range of temperatures controlled by a nitrogen jet (QUATRO from Novocontrol) with a temperature error of 0.1ºC, during every single sweep in frequency.

3. RESULTS

3.1. Dielectric spectra analysis

In order to get information about the behavior of the ionic conductivity and diffusion process of mobile carriers, electrochemical impedance spectroscopy measurements were performed on several solid acid compounds of cesium phosphate salts-doped. These compounds are labeled as CsP, CsP-Rb, CsP-Ba, CsP-S, CsP-W, and CsP-Mo, respectively.

The data have been analyzed in terms of the dielectric permittivity $\varepsilon^* = \varepsilon' - j\varepsilon''$, where the real part of conductivity σ' is obtained from imaginary ε'' part, as a pure ohmic conduction, through the expression $\varepsilon''=\sigma'/(\varepsilon_0\omega)$. Here, ε_0 y ω are the vacuum permittivity and the angular frequency of the applied electric field respectively.

In the Fig. 1 it is show the experimental data of conductivity as a function of the frequency at several temperatures. The conductivity σ' is characterized by a *plateau* in the high frequency range, and its value tends to a constant corresponding to the direct-current conductivity (σ_{dc}) of the sample. Deviation from σ_{dc} in the spectrum of the conductivity in the range of low frequencies is due to the EP effect resulting from the blocking electrodes, produced by mobile charge accumulation.[19,20]

The conductivity also exhibits a phenomenon of dispersion that obeys a behavior described by Jonscher law,[17,18] $\sigma(\omega) = \sigma_{dc} + \sigma_{ac}$, being σ_{dc} the *dc* conductivity mentioned before, and the alternate-current conductivity $\sigma_{ac} = A\omega^{m}$, where A is a factor dependent of the temperature and m , for an ideal Debye dielectric and ideal ionic type crystals, is 1 and 0, respectively. Experimental data of the conductivity were fitted to the Jonscher law and the parameters are shown in the Table 1. As we can see in Figure 1, only for low temperatures (below transition temperature) we have observed three different regions perfectly identified. The region of electrode polarization (EP), the region where the dc-conductivity will be determined (Cond), and the region of subdiffusive conductivity (SD).[26] In our work the values fitted for the parameter m are between 0.4 and 1 for all the samples, except in case of sample CsP-S where the value was 0, corresponding to an ideal ionic type in all the range of temperatures. For the other samples, the values obtained from the fit in the high frequency region can be due to the reorientation motion of dipoles and more likely to the motion of the localized charges, which are dominant over the dc-conductivity.[27]

Table 1. Jonscher parameters obtained by fitting $\sigma(\omega) = \sigma_0 + A\omega^m$ to conductivity data, for some indicated temperature in all studied samples.

CsP	**σ_{dc} [S cm]**	**A**	**m**	**CsP-Mo**	**σ_{dc} [S cm]**	**A**	**m**
T=150°C	1.45×10^{-6}	2.36×10^{-10}	0.59	**T=150°C**	4.04×10^{-6}	2.80×10^{-10}	0.63
T=180°C	4.04×10^{-6}	4.38×10^{-11}	0.70	**T=180°C**	1.12×10^{-5}	2.30×10^{-10}	0.67
T=210°C	1.66×10^{-2}	0	0	**T=210°C**	1.13×10^{-3}	0	0
T=240°C	3.79×10^{-2}	0	0	**T=240°C**	4.55×10^{-4}	0	0
CsP-Rb	**σ_{dc} [S cm]**	**A**	**m**	**CsP-S**	**σ_{dc} [S cm]**	**A**	**m**
T=150°C	3.23×10^{-7}	3.67×10^{-10}	0.46	**T=150°C**	1.43×10^{-3}	0	0
T=180°C	2.28×10^{-6}	6.78×10^{-10}	0.48	**T=180°C**	2.96×10^{-3}	0	0
T=210°C	8.51×10^{-3}	0	0	**T=210°C**	5.31×10^{-3}	0	0
T=240°C	2.35×10^{-2}	0	0	**T=240°C**	8.74×10^{-3}	0	0
CsP-Ba	**σ_{dc} [S cm]**	**A**	**m**	**CsP-W**	**σ_{dc} [S cm]**	**A**	**m**
T=150°C	9.31×10^{-5}	1.24×10^{-8}	0.65	**T=150°C**	6.90×10^{-7}	2.08×10^{-13}	0.99
T=180°C	2.85×10^{-4}	5.67×10^{-8}	0.53	**T=180°C**	3.15×10^{-6}	3.54×10^{-13}	0.98
T=210°C	1.70×10^{-3}	0	0	**T=210°C**	3.38×10^{-4}	0	0
T=240°C	2.75×10^{-3}	0	0	**T=240°C**	3.04×10^{-4}	0	0

In the Fig. 1 it can be observed the temperature variations of the conductivity. Also, at low temperatures σ_{ac} depends notably on the frequency and this effect disappears when the temperature increases. The emergence of a plateau associated with *dc* conductivity curves shifts at low temperatures and is little remarkable for CsP-S and CsP-Rb samples.

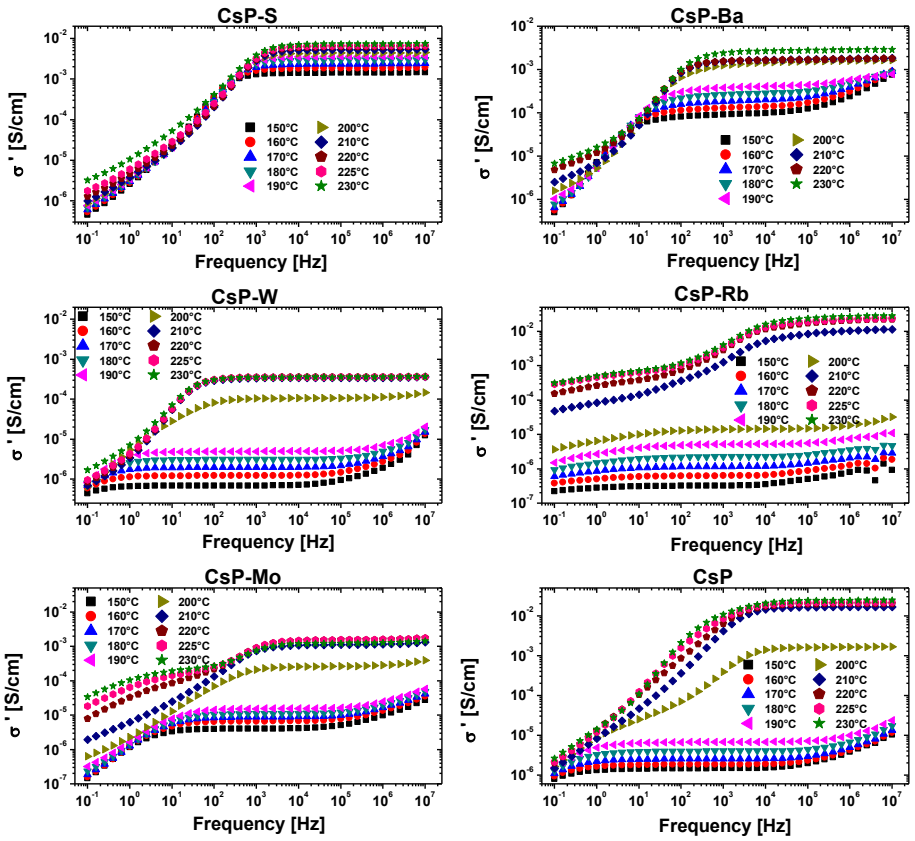

Figure 1. Bode diagram for the real part of the conductivity in the temperature range from 150ºC to 230ºC, for all the samples studied.

A close inspection of Fig. 1 shows a change in the behavior of the conductivity around 200ºC, for most samples except for CsP-S. For example, a jump between low (150 to 190ºC) and high temperatures (200 to 230ºC) is revealed for the salts CsP, CsP-Rb, CsP-Mo and CsP-W. However, this gap is very small in the sample CsP-Ba. These differences in behavior are due to the presence of a superprotonic phase transition, such as have been also observed in a great number of solid acid sulfates and selenates, where the proton conductivity jumps by 3-4 orders of magnitude.[28-31]

Figure 2 shows the plots of ε', ε" and loss tan δ as a function of the frequency for a set of temperatures and for two protonic conductors, CsP-W and CsP-S. In the rest of the samples, a behavior similar to that of CsP-W is observed.

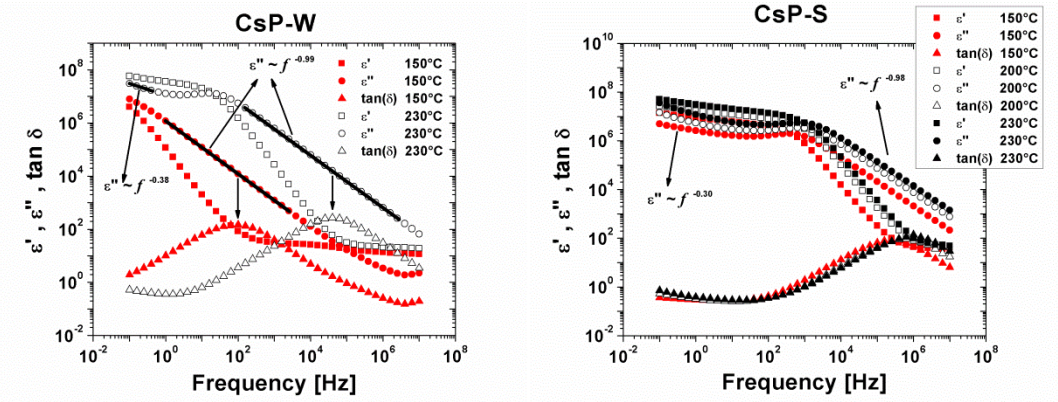

Figure 2. Real part ε' (squares) and imaginary part ε" (circles) of the complex dielectric permittivity ε*, and loss tan δ (triangles) for two samples at several temperatures. Left: CsP-W sample at 150 ºC and 230ºC. Right: CsP-S sample at 150 ºC, 200ºC and 230ºC.

The Fig. 2 also shows that the dependence at high frequencies of ε", is almost linear with a slope very close to unity. This represents the electrical conduction contribution to the dielectric loss, and in this case is due to the *dc*-conductivity corresponding to the proton conduction.[10] For intermediate frequencies, the maximum observed can be explained as a Cole-Cole type relaxation and is due to the macroscopic polarization of the ionic charges in the alternating electric field. This behavior is defined by a relaxation time τ_{EP}, a shape parameter of process α, and a dielectric relaxation strength characterized by the parameter M, which depends on temperature and the material properties. In a first approximation, the relaxation time would be understood as an effective relaxation time where cation and anion can be mobile.

At low frequencies, the dependence is again linear, but with a slope less than unity; that is an evidence of a dependence of the type $\varepsilon'' = \sigma'/(\varepsilon_0\,\omega^s)$, with $s \leq 1$ (see signal arrows in the Fig. 2, with s=0.38 (left) and s=0.30 (right)). When the system is an ion conductor the exponent s is near to 1, while $s<1$ is an indication of diffusion limited hopping.[10] Here, the parameter σ' is related to some kind of conductivity (i.e. impurities or like-charges).[10,13-16] This can be due that at very low frequencies, once the electrode polarization has almost completely build-up, there is still a remaining conductivity because of some very slow ions, most probably at interface, imply a surface interaction at ionic conductor ($M^+ X^-$) /insulator heterojunction.[6]
When the temperature increases, the maximum of ε'' shifts to higher frequencies, such is shown in Fig. 2. A similar effect is observed for the other samples, although some differences in the behavior exist. For example, in the CsP-W sample (see Fig. 2-left), the peaks at 150ºC and 230ºC are shifted a frequency interval of around three decades, while in the CsP-S sample (see Fig. 2-right), the maxima at 150ºC, 200ºC and 230ºC are separated less than one decade.
When ω is greater than a cut-off value ω_{cut} , the real part of the dielectric permittivity ε' tends to a limit value ε_∞, which corresponds to the static permittivity value ε_s, in the high frequency range (where the conductivity is considered constant), while the imaginary part of the permittivity ε" changes according to $\varepsilon''=\sigma_{dc}/(\varepsilon_0\omega)$.
A maximum in tan δ appears when the complex dielectric permittivity ε" varies with frequency as $\varepsilon'' = \sigma/(\varepsilon_0\omega)$ which indicates that this peak is due to a conduction process. At this frequency the parameter σ_{dc} of the samples is obtained.

In Fig. 2 it is represented the imaginary part of the permittivity ε", in order to observe how the frequencies of the peaks are related to different relaxation behavior and therefore obey another processes. The maxima of ε" display a Debye behavior, due to the EP effect. These peaks are shifted to frequencies lower than those of the conductivity (see Fig. 1) and characterize the polarization processes. Their frequencies allow to obtain the time in which the above mentioned processes begin to develop in the acid salts studied.
Taking into account the above comments the dielectric loss spectra is modeled as a function of the angular frequency by mean of the piece-wise function given as,

$$\varepsilon''(\omega) = \begin{cases} \mathrm{Im}\left(\varepsilon_S + \dfrac{\Delta\varepsilon_{EP}}{1+(j\omega\tau_{EP})^{\alpha}} + \dfrac{\sigma'}{\varepsilon_0\omega^{s}}\right) & \omega \le \omega_{cut} \\ \dfrac{\sigma_{dc}}{\varepsilon_0\omega} & \omega \ge \omega_{cut} \end{cases} \qquad (1)$$

where $\Delta\varepsilon_{EP} = \varepsilon_{EP} - \varepsilon_S$, with ε_{EP} being the dielectric constant with EP. The quantity τ_{EP} is the EP macroscopic relaxation time, involving charging/discharging of the electrode double layer capacitance, and it is proportional to sample thickness. It is usually defined in terms of the bulk resistance R_B and the interfacial capacitance C_{EP} as $\tau_{EP} = R_B C_{EP}$.[22,32] The exponent α, is the width relaxation and *j* is the imaginary unity ($j = \sqrt{-1}$). The low frequency range ($\omega<\omega_{cut}$) is made-up by a Cole-Cole macroscopic polarization term, and is due to the movement of ions plus a conductive term that might arise from some residual diffusion and persists once the electrode polarization has built-up. The high frequency region ($\omega>\omega_{cut}$) represents the contribution to the dielectric loss to the protonic conductivity by means of the expression, $\varepsilon''=\sigma_{dc}/(\varepsilon_0\omega)$. Then the cut-off angular frequency ω_{cut}, is the frequency at which the electrode polarization is practically irrelevant, and the sample tends to a behavior quasi-ideal respecting the protonic conduction.

Once the conductivity values have been obtained from Bode plots of Fig. 1, their variation with the temperature is observed in Fig. 3. An overview of these data shows an increase, by several orders of magnitude in the conductivity, associated to an ionic phase transition from a low-conductivity (protonic phase) to a high-conductivity phase (superprotonic phase). Analogous behavior has been observed in the study of similar compounds.[33]

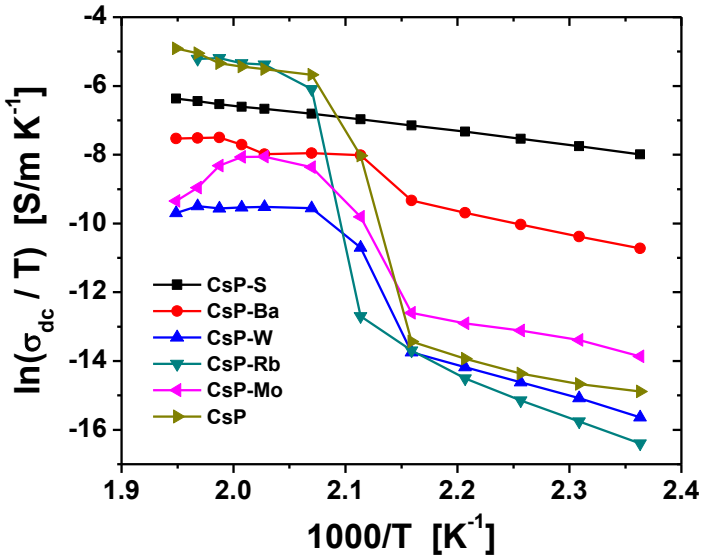

Figure 3. Temperature dependence of the direct-current conductivity (σ_{dc}) for all the samples studied in all the range of temperatures.

The Fig. 3 shows that the conductivity rises with the increase in the temperature and there is a steep change in the conductivity at $T = T_{sp}$, being T_{sp} the temperature at which occurs the superprotonic phase transition. This temperature depends of salt dopant and occurs in the range between 200 and 215ºC in humid conditions for most of the samples, except for the dopant salt of CsP-S. In polycrystalline sample Cs-P, the transition occurs between 200 and 210ºC and similar results have been observed by Otomo, *et al.* in the study of protonic conduction of CsP and its composite with silica.[6] Note that this jump is four orders of magnitude for the CsP sample, three orders for the doped salt CsP-Mo, and two orders of magnitude for CsP-W sample. Moreover, in the comparison of the behavior of CsP-Ba and CsP-Rb, the latter presents an increase in conductivity by about four orders of magnitude, while for CsP-Ba this growth is just only one order of magnitude. The CsP-S sample does not have the same behavior as the other salts, just as the transition between low-temperature monoclinic phase to high-temperature tetragonal (instead cubic phase) appears around of 141ºC in $CsHSO_4$.[34] . This temperature is outside our range of measurements. Taking into consideration the EDX study the composition suggested for the sample CsP-S is that the mixture will be basically made of Cs_2SO_4 with some impurity due to CsH_2PO_4. The best fit corresponds to 0.96 Cs_2SO_4-0.04CsH_2PO_4, this means that sample named CsP-S is formed mostly by Cs_2SO_4. According to these results, we can think that the conductivity values correspond to the superprotonic transition in the heating regime, because we are started our experimental study from 150ºC. This affirmation is in agreement with the results of the study of Ponomareva et al.,[49,50] where the partial HSO4-substitution in CsH_2PO_4 produce a solid solutions of the resultant $(CsH_2PO_4)_{1-x}$ $(CsHSO4)_x$ compounds with different behavior depending of the amount of CsHSO4. When the amount of $CsHSO_4$ is higher, then the superprotonic phase transition, due to the rearrangement of the sulfate-phosphate tetrahedral, becomes, broader and shift to lower temperature around 130ºC at 10% and disappear around 15% of $CsHSO_4$. On the other hand, investigations carried out by Ponomareva et al[49,50], in pure polycrystalline $Cs_3(HSO_4)_2H_2PO_4$ clearly demonstrate that temperature of the superprotonic phase are around 137ºC in the heating regime and about 113ºC on cooling, both temperatures are

below our range of temperature. Therefore, the superprotonic phase transition could have been produced at temperatures below 150 ºC for CsP-S salt, since the measurements start above this value and the jump cannot be seen. Also Haile et al.,[28] in identical compounds to Ponomareva et al.[49], showed a temperature transition around 119ºC. EDX measurements of our compound CsP-S shows that relations between compositions of Cs/P and Cs/S were 51 and 1.85, respectively, that is to say that the amount of CsH_2PO_4 in the mixed compounds was around 4%. Therefore, we think that the superprotonic phase transition of CsP-S samples have been produced at temperatures below 150 ºC, because the effect of the CsP salt (around 4%) is very smaller in comparison with the amount of the Cs_2SO_4 in the mixture.

Table 2 Values of activation enthalpy (**ΔH**), entropy (**ΔS**) and activation energy ($\boldsymbol{E_a}$) for all samples studied. Two set of values are given, under the transition ($T<T_{sp}$) and above the transition ($T>T_{sp}$).

Salt	**$T<T_{sp}$**			**$T>T_{sp}$**		
	ΔH (kJ/mol)	**ΔS** J mol^{-1} K^{-1}	$\boldsymbol{E_a}$ (kJ/mol)	**ΔH** (kJ/mol)	**ΔS** J mol^{-1} K^{-1}	$\boldsymbol{E_a}$ (kJ/mol)
CsP	62.4±2.1	15±2	66.2±2.0	16.2±1.5	12.5±1.2	17.8±2.5
CsP-S	—	—	—	39.0±0.5	23.3±1.8	43±0.6
CsP-Ba	54±3	45±3	58±3	28.9±1.8	11±2	31.1±2.3
CsP-W	77±4	51±2	80±4	2.5±0.3	58±7	4.3±0.4
CsP-Rb	117.4±2.5	146±4	120±2.4	17.4±2.1	99±5	19±2
CsP-Mo	50±2	1.5±1.0	53±2	7±1	18±4	8±1

In order to continue with the analysis of the conductivity of the salts, the Eyring's rate theory is used,[35] where the conductivity varies with temperature through the expression

$$\sigma = C_0 T \exp\left(-\frac{\Delta G_a}{RT}\right). \qquad (2)$$

Here $\Delta G_a = \Delta H_a - T\Delta S_a$ is the free energy associated with the energy barrier for the ionic transport. The pre-factor C_0, is a reference value and R is the constant of gases. Namely the diffusion of ions is thermally activated, and the energy ΔG_a involve the formation of the activated complex linked to ion hopping. Thus ΔH_a and ΔS_a are the activation enthalpy and entropy, respectively. Calculation of ΔH_a is obtained from the slope of the plot $\ln(\sigma/T)$ vs $1/T$ (Fig. 3), and ΔS_a is estimated from the y-intercept from this plot. In the estimation of activation entropy C_0 is considered equal to one, and is taken the same for the protonic and superprotonic phase. The activation energy E_a is calculated from the Arrhenius expression in the conductivity $\sigma = A\exp(-E_a/RT)$, where A is a coefficient independent of temperature. Values of these quantities are shown in the Table 2. Notice that for the sample CsP-S the activation enthalpy and the entropy are obtained for the only one phase. For these data is observed that for most samples, the activation

enthalpy decreases from one phase to the another. In addition, the values of ΔS_a increase for the CsP, CsP-Mo and CsP-W samples, suggesting that higher value of activation entropy is associated with the higher conductivity (order-disorder transition), and with the structural change from the monoclinic to cubic phase (disorder-order transition).
It is also observed for all samples that the activation energy E_a decreases as temperature increases. This means that in the superprotonic phase, the barrier energy is small compared to protonic phase and hence the conductivity rises. Finally activation energies of pure CsP obtained in low conductive phase (66.2 kJ mol =0.69eV) are significantly smaller than the previous values reported by Baranov *et al*.[5] (around 0.95eV≅91 kJ/mol), whereas the value obtained in the superprotonic phase was 17.8 kJ/mol (0.19eV) also smaller than 0.30eV and 0.29 eV, reported by Baranov *et al*.[5]and Ortiz *et al*.,[7,8] respectively.
However, our values in low conductive phase are higher than the values reported by Otomo *et al*.[6] (around 0.45eV), while for high conductive phase the value was 0.19eV smaller than that found by Otomo *et al*. (0.37eV). Such differences can be related with the humidity conditions. In our experimental procedure, the samples are below a flux of 30% N_2/H_2O gaseous mixture at atmospheric pressure, while in Otomo *et al*. the flux was 30% Ar/H_2O. Finally, the activation energy obtained for the compound CsP-S was 43kJ/mol (0.49eV) about 1.6 times higher than the value found by Ponomareva et al.[50]. These differences could be due to differences in the Cs/P and Cs/S ratios of the compound and the humidity of the air flux

3.2. Electrode polarization analysis

In the experimental assembly in wet conditions procedure, a sample sandwiched between two graphite sheets was introduced between two porous stainless steel circular electrodes of 10 mm diameter completely blocking electrodes. Owing to an EP phenomenon, a suitable analysis should be carried out. Although different EP models have been established to determine the mobility and ionic concentration of charge carriers using impedance spectroscopy measurements,[10,13,14,36-40] the Klein *et al.* model method[10] will be followed. It is based on Coelho model,[36] where the ionic charge density and the ion mobility are obtained from measurements of $\tan\delta$ in ionic conductors and polymeric membranes.[11,38,41-43]

On the other hand, based on the EP model Fragiadakis *et al.*,[39,40] they explain the conduction mechanism proffering an expression to separate the ionic conductivity into the contribution of mobile ion concentration and ion mobility, as a function of the ion content and the dielectric constant measured experimentally. In this equation the authors provides much better fits to the data of complex permittivity, reproducing the shape of the curves over the entire frequency range. Although, in these EP model the authors do not need to split the imaginary part of the dielectric permittivity in the low and high frequency regions, in this work we make use of a piecewise function which is Debye at high frequencies and Cole-Cole at low frequencies. Such function allowed us to fit the experimental data more accurately than the Klein *et al.*[10] method. A theoretical justification for this procedure is given in Híjar *et al.*[44]

Unlike that in the Klein model, the dependence of the complex dielectric permittivity on frequency is represented by a single Debye relaxation, in this work it is expressed in terms of a piecewise Cole-Cole function by mean of Eq. (1), where the real and imaginary parts are, respectively

$$\varepsilon' = \varepsilon_S + \frac{\Delta\varepsilon_{EP}\left[1+(\omega\tau_{EP})^{\alpha}\cos\left(\frac{\pi\alpha}{2}\right)\right]}{1+2(\omega\tau_{EP})^{\alpha}\cos\left(\frac{\pi\alpha}{2}\right)+(\omega\tau_{EP})^{2\alpha}} \tag{3}$$

and

$$\varepsilon'' = \frac{\Delta\varepsilon_{EP}(\omega\tau_{EP})^{\alpha}\sin\left(\frac{\pi\alpha}{2}\right)+\frac{\sigma_{dc}}{\varepsilon_0\omega}\left[1+2(\omega\tau_{EP})^{\alpha}\cos\left(\frac{\pi\alpha}{2}\right)+(\omega\tau_{EP})^{2\alpha}\right]}{1+2(\omega\tau_{EP})^{\alpha}\cos\left(\frac{\pi\alpha}{2}\right)+(\omega\tau_{EP})^{2\alpha}}. \tag{4}$$

In Eq. (4) the contribution of the conductivity σ' at low frequencies is omitted, because it is negligible regarding the σ_{dc} term. From Eqs. (3) and (4) it can be obtained the loss $\tan\delta = \varepsilon''/\varepsilon'$, as

$$\tan\delta = \frac{\Delta\varepsilon_{EP}(\omega\tau_{EP})^{\alpha}\sin\left(\frac{\pi\alpha}{2}\right)+\frac{\sigma_{dc}}{\varepsilon_0\omega}\left[1+2(\omega\tau_{EP})^{\alpha}\cos\left(\frac{\pi\alpha}{2}\right)+(\omega\tau_{EP})^{2\alpha}\right]}{\varepsilon_S\left[1+2(\omega\tau_{EP})^{\alpha}\cos\left(\frac{\pi\alpha}{2}\right)+(\omega\tau_{EP})^{2\alpha}\right]+\Delta\varepsilon_{EP}\left[1+(\omega\tau_{EP})^{\alpha}\cos\left(\frac{\pi\alpha}{2}\right)\right]}. \tag{5}$$

If α=1 in the Eq. (5), the expression for the tan δ of Ref.[10] is recovered. Since the σ_{dc} term has no effect on the tan δ peak, this can be neglected, and then the Eq. (5) is written as,

$$\tan\delta = \frac{(\omega\tau_{EP})^{\alpha}\sin\left(\frac{\pi\alpha}{2}\right)}{1+(\omega\tau_{EP})^{\alpha}\cos\left(\frac{\pi\alpha}{2}\right)+\frac{(\omega\tau_{EP})^{2\alpha}}{M}}, \tag{6}$$

with $M = \varepsilon_{EP}/\varepsilon_S$. If α=1, then Eq. (6) is reduced to Coelho model, where EP behavior is represented by a single Debye relaxation.

Figure 4 shows the tan δ as a function of the frequency for all the samples studied in all the range of temperatures. A maximum in the curves at each temperature can be observed, and it shifts abruptly to high frequencies as the temperature increases. In the beginning, an increase in the temperature produces a growth in maximum intensity, but its intensity decreases when the transition temperature T_{sp} (around 210ºC) is reached, and then gradually rises with the increase in temperature. This can be seen for the salts: CsP, CsP-Mo, CsP-W, CsP-Rb and CsP-Ba. The shift in the maxima is indicative of the aforementioned superprotonic transition phase (matching with polymorphic structural phase transition). This transition arises in most of the samples except for the salt CsP-S, because it could have been happened at temperatures around 150ºC.[25,34]

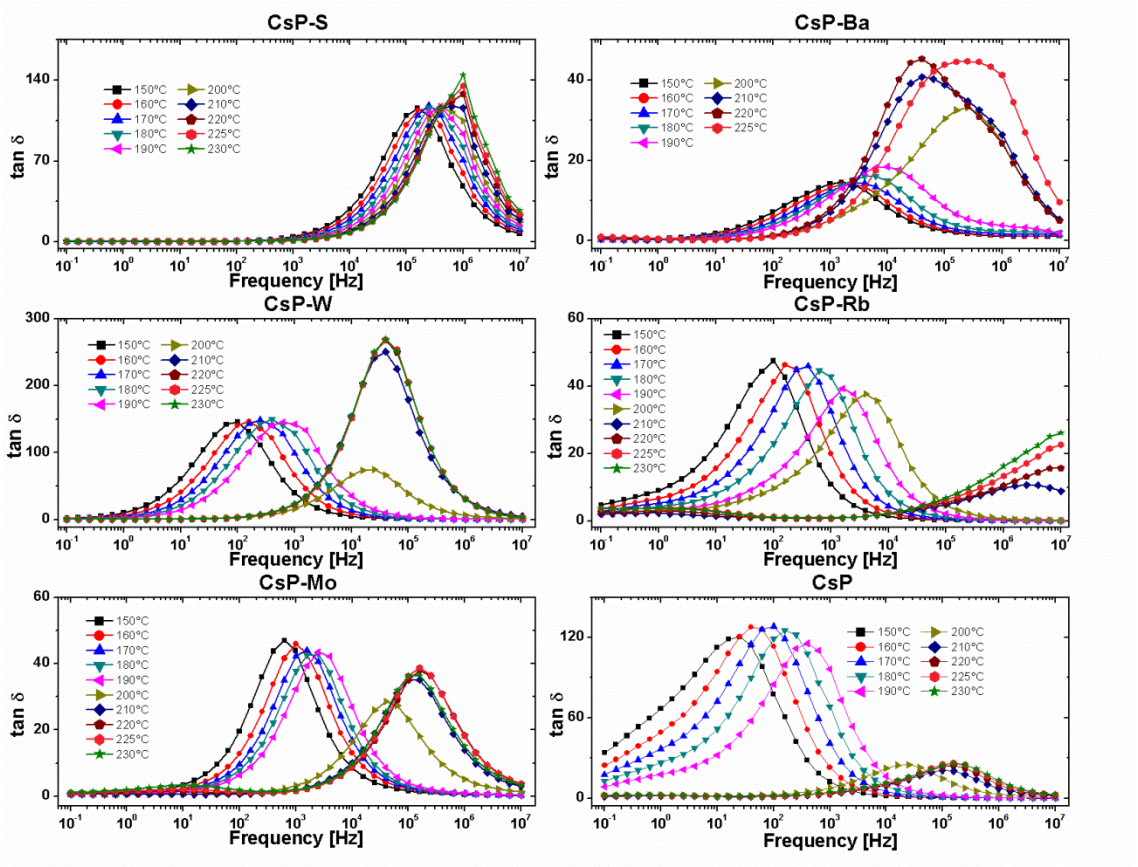

Figure 4. Tan δ vs. frequency in all the range of temperatures for each one of salts studied.

When it is compared the intensity of the loss tangent of CsP pure salt with those that are doped, several effects are observed. For example, the addition of Rb (in CsP-Rb sample) instead of Ba (in CsP-Ba sample) barely displays the maxima in the loss tangent at high temperature transition (see Fig. 4). However, in the case of salt with Ba, the inclusion of atoms larger than Rb, produces peaks much wider; this means that the width frequency changes in one decade.

Equation (5) has been used to fit the experimental data shown in Fig. 4 to provide the estimation for M, τ_{EP} and α, for three values of the temperature (150ºC, 200ºC and 230ºC) The values of these parameters are given in Table 3.

Table 3. Parameters M, τ_{EP} and α on equation (5) for some temperatures, from fitting the experimental data for tan δ.

Salt	T=150ºC			T=200ºC			T=230ºC		
	M	τ_{EP} [s]	α	M	τ_{EP} [s]	α	M	τ_{EP} [s]	α
CsP	3.86E+05	4.58E+00	9.97E-01	1.15E+04	9.06E-04	9.87E-01	1.42E+04	1.24E-04	9.86E-01
CsP-S	1.64E+05	4.39E-04	9.98E-01	1.60E+05	1.46E-04	9.98E-01	2.90E+05	1.20E-04	9.97E-01
CsP-Ba	7.81E+03	1.08E-02	9.71E-01	5.82E+04	1.88E-04	9.86E-01	1.01E+06	7.31E-04	9.87E-01
CsP-W	3.66E+05	1.17E+00	9.98E-01	7.97E+04	2.37E-03	9.96E-01	6.19E+05	3.20E-03	9.99E-01
CsP-Rb	1.46E+04	2.07E-01	9.97E-01	2.26E+04	6.80E-03	9.92E-01	9.32E+06	4.40E-06	9.78E-01
CsP-Mo	9.16E+05	9.59E+00	9.96E-01	1.56E+04	1.14E-03	9.84E-01	1.86E+04	1.58E-04	9.84E-01

The α value is close to the unity, meaning a limit value in the Cole-Cole model corresponding to a Debye behavior. It is also observed that the relaxation time τ_{EP} and the parameter M, depend on the temperature. In Fig. 5, it can be seen the fitting for three materials CsP, CsP-Ba and CsP-Mo at two temperatures, one below transition (150ºC) and the other above the transition (220ºC).

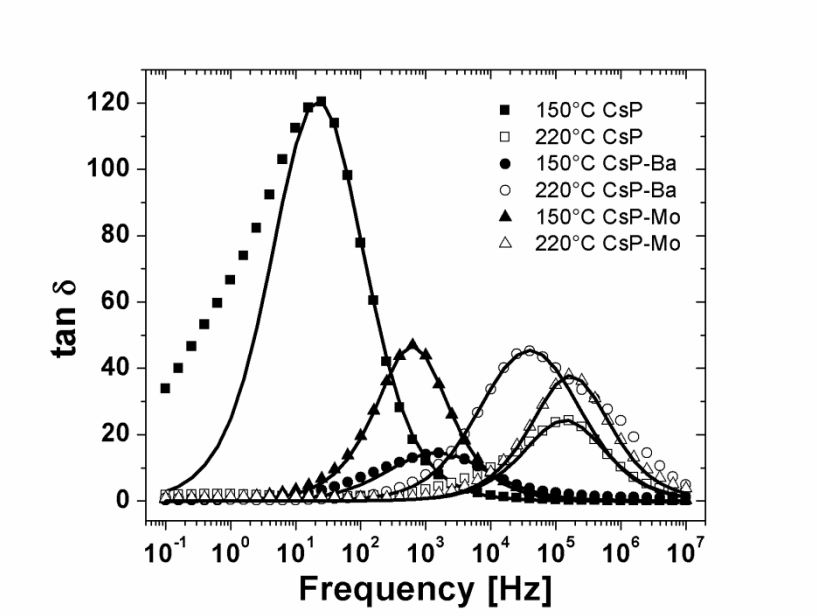

Figure 5. Tan δ as a function of the frequency at 150ºC and 220ºC for CsP (squares), CsP-Ba (circles) and CsP-Mo (triangles). The solid lines indicate the convolution of Eq. (5) in the peak of tan δ at higher frequencies.

The curves shown in Fig. 4, display peaks corresponding to the maxima in tan δ (Eq. (5)) and are associated with the plateau of the real part of the conductivity observed in the Bode diagrams (see Fig. 1). Their corresponding values in frequency are related with the parameters M and τ_{EP} as

$$\omega_{\max}^{\tan\delta} = \frac{M^{\frac{1}{2\alpha}}}{\tau_{EP}}, \tag{7}$$

where the EP relaxation time, when the electrode polarization is completely build-up, is[45,46]

$$\tau_{EP} = \frac{\varepsilon_{EP}\varepsilon_0}{\sigma_{dc}}. \tag{8}$$

The quantity *M* is also expressed as $M=L/2L_D$, and the parameters τ_{EP} and ε_{EP} are related to *M* trough expressions, $\tau_{EP} = M\tau$ and $\varepsilon_{EP} = M\varepsilon_S$, being τ the relaxation time also

defined as $\sigma = \frac{\varepsilon_S}{\sigma_{dc}}$ where ε_S is the dielectric permittivity of the sample. The parameter L is the thickness of the sample (i.e. electrode separation when the sample is sandwiched to take the measurements) and L_D is de Debye length, defined as

$$L_D = \sqrt{\frac{\varepsilon_S \varepsilon_0 kT}{q^2 n}}, \tag{9}$$

where k is the Boltzmann constant, T the absolute temperature, q is the ion charge and n the mobile charge density.
Considering that cation and anion have approximately the same mobility μ, the conductivity σ_{dc} is expressed in terms of n and μ as,[11]

$$\sigma_{dc} = nq\mu . \tag{10}$$

Using the equations of τ_{EP} and ε_{EP} in terms of M together with Eq. (8), the mobility is determined as,

$$\mu = \frac{qL^2}{4M\tau_{EP}kT} \tag{11}$$

and then taking into account the Einstein relation for ion diffusivity together with Eqs. (7)-(11), it is calculated the diffusion coefficient of the protons as

$$D = \frac{L^2}{4M\tau_{EP}}. \tag{12}$$

The Eq. (12) allows determining the ion diffusivity in terms of parameters M, τ_{EP} and L.

From Eqs. (9) and (12), the ionic charge density is,

$$n = \frac{\sigma_{dc}kT}{Dq^2} \tag{13}$$

The values for diffusivity D using Eq. (12) and charge density n with Eq. (13), are shown in Figs. 6 and 7 respectively, as a function of the temperature. In the Fig. 6, a similar effect in diffusivity to that observed in conductivity (see Fig. 3), is appreciated. The diffusivity rises as the temperature increases, and an abrupt change in the behavior appears around 200ºC for most of the samples. It can be related with the superprotonic phase transition, which is happening in the range between 200-210ºC.

This transition is due to the change of the crystallinity of the salts, where in the low-temperature conductive phase the diffusion coefficient is about 10^{-12} m^2/s at 150ºC, and in the high-temperature superprotonic phase is about 10^{-6} m^2/s at 220ºC for CsP.
This structural change is explained considering that under room temperature, there is a network where PO_4^{-3} oxyanions are linked via O–H··O bonds forming $H_2(PO_4)^-$ layers and Cs is situated between these layers. When the temperature is increased there is a reorientation of the oxyanions giving a cubic phase.

The proton conductivity of CsP at high temperatures takes place following two different and competing mechanisms: diffusion (vehicle transport) and Grotthuss mechanism. In the first one, the fast proton hopping is followed by a slow repositioning of the oxyanions, whereas the reorientation of the PO_4 group is not necessary in the Grotthuss mechanism.[47] At high temperatures, the PO_4 tetrahedron reorientation (the slowest process) is favored, resulting in an improvement of the diffusion coefficient of protons. Similar results are found for the other salts, and in the CsP-S sample the conductivity and the diffusion coefficient are very high (around 10^{-1} S/m for conductivity and 10^{-8} m^2/s in case of diffusivity), because it is already in the superprotonic phase.

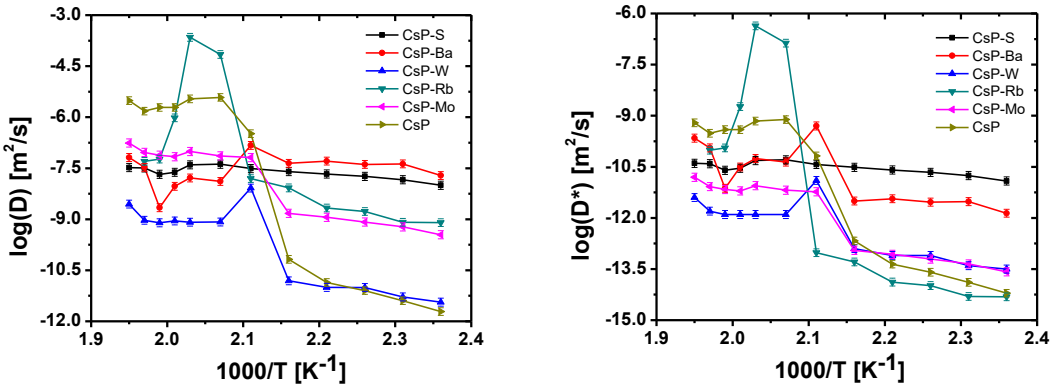

Figure 6. Left) Behavior of diffusion coefficient calculated following the EP model by means of Eq. (12). Right) Diffusion coefficient (D*) after correcting the number density using the factor of proportionality, $N = \frac{n_{tot}}{n_0}$.

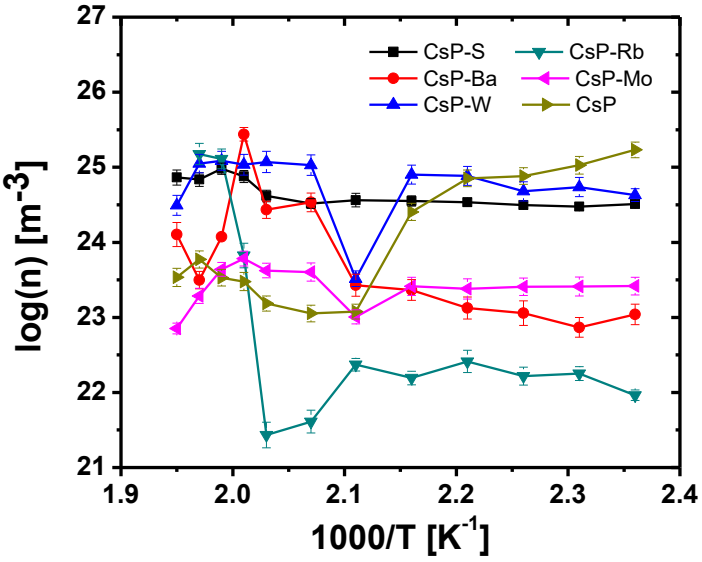

Figure 7. Temperature dependence of free-ion number density n calculated from the EP effect using the Klein *et al.* model for all the samples studied.

From the results shown in Fig. 7, it can be seen that the proton concentration is fairly constant in the protonic phase (low-temperature phase) varying from $9.18x10^{21}$ m^{-3} to $1.7x10^{25}$ m^{-3}. Between 200-210ºC the concentration decreases and it can be due to the change of crystallinity involving a reorientation of crystals of the pellets. When the temperature increases above 210ºC, a normal tendency to follow the same behavior than in low temperature phase is observed, increasing for all the samples in the high-temperature cubic phase. For example, the concentration of charge carrier density changes from $9.18x10^{21}$ m^{-3} for CsP-Rb in monoclinic phase to around of $1.5x10^{25}$ m^{-3} in the case of cubic phase. Similarly, for CsP-Ba the change is about three orders of magnitude between monoclinic and cubic phase transition (from $7.37x10^{22}$ m^{-3} to around $2.75x10^{25}$ m^{-3}). However, it cannot be appreciated any change for the samples CsP-Mo, CsP-W and CsP-S where the only change is observed through the transition temperature interval. In the case of CsP, the free-ion number density decreases from $1.71x10^{25}$ m^{-3} to $1.23x10^{23}$ m^{-3}. The values of mobile ion concentration is surprisingly low than stoichiometric calculations where the total concentration of protons, (n_{tot}) is around 10^{28} m^{-3} at room temperature. Which yields a dissociation degree of roughly 10^{-3} at low-temperature phase and 10^{-5} for the super protonic phase. These values are quite similar to those found for other polyelectrolytes.[39,40,48]

Our analysis based on electrode polarization, only reflects the diffusivity of free ions. Our calculations gave a quantity of free ion concentration, *n*, lower than the total amount calculated theoretically, n_{tot}, being evident that these results overestimated the ion diffusivity. In general, the free ion concentration can be described by the Arrhenius equation $n=n_0 \exp(-E_{dis}/k_BT)$, where E_{dis} is the dissociation energy and n_0 the number density in the high temperature limit at which we can assume a complete dissociation. As it is known the electrode polarization model is based on the Debye-Hückel theory and therefore can be expected that this model fails in the case of high ionic concentrations. To solve this contradiction, we have followed the same line of reasoning that Wang *et al.*[23,24], correcting the number density using the factor of proportionality, $N = \frac{n_{tot}}{n_0}$ and its reciprocal $\frac{1}{N} = \frac{n_0}{n_{tot}}$ to correct the diffusivity. In this case n_{tot} is the total ion number density calculated theoretically from the preparation of the samples. In this way the corrected diffusivity will be

$$D^* = D\frac{n_0}{n_{tot}} \qquad (14)$$

Where *D**, is the diffusivity after correction and *D* is the value obtained from eq. (12). Figure 6-right shows the corrected diffusivities. The values obtained after correction are more consistent with the general protonic diffusivity values observed in polymers.[22,23,24,39,40,48]

Alternative models have been used to calculate the average free ion diffusivity, *D*. One of them is the Macdonald-Trukhan model, where the diffusion coefficient of the protons is calculated through the expression,

$$D = \frac{2\pi f_{max} L^2}{32(\tan\delta)^3_{max}}, \quad (15)$$

where f_{max} and $(\tan\delta)_{max}$ are the frequency and the amplitude of the EP tan δ maximum, and *L* is the sample thickness. In Eq. (14) the experimental values for f_{max} and $(\tan\delta)_{max}$ shown in Fig. 4 for all the samples studied, are introduced. The estimation of the diffusion coefficient at several temperatures are given in Table 4. Also in this table, the values calculated following the Eq. (12) obtained from the Klein model, are reported. From the comparison of these two models, it could be observed smaller values of diffusivity on Klein model, than in Macdonald-Trukhan description Eq. (15). However both values of the ion diffusivity are overestimated. It is known that the EP model yields reasonable ionic dissociation energy, but the obtained diffusivities are not in agreement with experiment, suggesting that the analysis of ion diffusivity and number density using the EP model should be considered with great caution, such as also have been observed by Wang *et al.*[23] From our results, it can be concluded that the EP model may only describe the dielectric response qualitatively, however the model tends to fail when quantitative values are considered. Based on these observations, we think that diffusivity analysis from EP model should be corrected, at least in the case of ionic conductors, solutions or polymers with high charge concentration, such as we are done. A thorough analysis of these differences is beyond the purpose of our work; however, a more complete study of it will be discussed later in another paper where the transition observed for the samples studied will be completely analyzed.

Table 4. Values of the average free ion diffusivity *D*, calculated from Klein model, Eq. (12), before corrections, and Macdonald-Trukhan model, Eq. (15).

Salt	**T=150ºC**		**T=190ºC**		**T=230ºC**	
	D (m^2/s) Eq. (12)	**D (m^2/s) Eq. (14)**	**D (m^2/s) Eq. (12)**	**D (m^2/s) Eq. (14)**	**D(m^2/s) Eq. (12)**	**D (m^2/s) Eq. (14)**
CsP	1.94×10^{-12}	1.6×10^{-10}	6.63×10^{-11}	7.6×10^{-10}	1.94×10^{-6}	1.3×10^{-6}
CsP-S	1.01×10^{-8}	3.2×10^{-7}	2.54×10^{-8}	6.7×10^{-7}	2.08×10^{-8}	4.2×10^{-7}
CsP-Ba	1.93×10^{-8}	6.5×10^{-7}	4.41×10^{-8}	2.0×10^{-6}	6.52×10^{-8}	2.1×10^{-6}
CsP-W	3.66×10^{-12}	2.5×10^{-11}	1.55×10^{-11}	1.6×10^{-10}	7.88×10^{-10}	1.7×10^{-9}
CsP-Rb	7.94×10^{-10}	7.3×10^{-10}	8.36×10^{-9}	2.1×10^{-8}	5.85×10^{-8}	4.0×10^{-8}
CsP-Mo	3.50×10^{-10}	4.8×10^{-9}	1.49×10^{-9}	5.7×10^{-8}	7.62×10^{-8}	2.6×10^{-6}

Finally, the values of the static permittivity ε_s can be estimated from EP model followed here[10] and from Anatoli Serghei description.[20] In the EP model ε_s is determined as

$$\varepsilon_s = \frac{\sigma_{dc}\tau_{EP}}{M\varepsilon_0}, \quad (16)$$

in terms of fitting parameters.

The Serghei procedure provides another method to calculate the static permittivity, ε_s. In this method the permittivity is expressed in function of the values of the onset of the EP (f_{ON}) and that corresponding to the frequency for the full development of EP (f_{max}). Both values are found from the curves of double logarithmic plot of σ" versus frequency, and are related with the static permittivity, ε_s. as

$$\varepsilon_s = \frac{\sigma_{dc} f_{max}}{2\pi\varepsilon_0 f_{ON}^2} \quad (17)$$

Table 5. Values from EP model (Eq. (16)) and from Serghei expression (Eq. (17)), for static permittivity on the indicated temperatures for all samples, respectively.

Salt	T=150ºC ε_S (Eq.15)	T=150ºC ε_S (Eq.16)	T=200ºC ε_S (Eq.15)	T=200ºC ε_S (Eq.16)	T=230ºC ε_S (Eq.15)	T=230ºC ε_S (Eq.16)
CsP	1.94E+02	1.04E+01	1.37E+03	1.75E+01	2.38E+03	6.89E+01
CsP-S	4.33E+01	2.56E+00	4.57E+01	3.30E-01	3.43E+01	6.79E+00
CsP-Ba	1.45E+03	4.20E+02	5.72E+01	4.47E+00	1.82E+01	2.53E+01
CsP-W	2.48E+01	1.23E+01	3.57E+01	1.20E+01	2.07E+01	1.01E+01
CsP-Rb	5.11E+01	5.75E+00	4.92E+01	1.04E+01	1.49E+01	3.16E+00
CsP-Mo	4.76E+02	4.57E+01	2.15E+02	5.28E+01	1.17E+02	2.26E+00

Fig. 8 shows the double logarithmic plot of imaginary part of conductivity versus frequency for CsP-S and CsP-Rb. Similar curves were obtained for the other samples. From these figures we can obtain at each temperature the frequency values of the onset (f_{ON}), and the frequency for the full development of electrode polarization (f_{max}), which permit us obtain the static permittivity following the Eq. (17). The values of ε_s calculated following the EP model and Serghei method, are shown in Table 5. A close inspection of these results indicates that static permittivity decrease when temperature increases, and the values obtained following the Serghei expression are smaller than that obtained by using the Eq. (16). Both calculations are different that the values found experimentally.

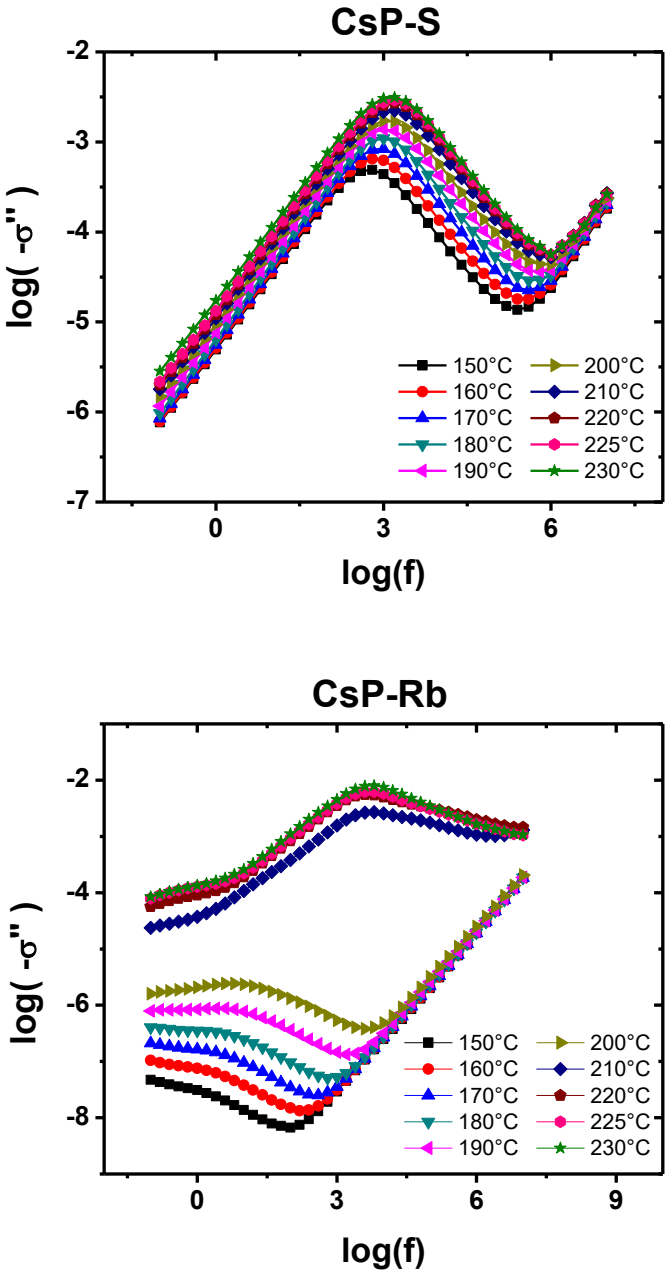

Figure 8. Double logarithmic plot of σ" versus frequency in the complete range of temperatures studied for CsP-S and CsP-Rb.

A close inspection of Figure 8 shows that the imaginary part of the conductivity, similar to observed with the real part of the conductivity, rises with the increase in the temperature and there is a steep change in the conductivity at the temperature at which occurs the superprotonic phase transition, T_{sp}. This temperature depends of salt dopant and occurs for the sample CsP-Rb in the range between 200 and 210ºC, in humid conditions. Note that the jump observed for log σ" for the values of the maximum and minimum is about four orders of magnitude for CsP-Rb sample. Finally, the CsP-S

sample, such we are commented before, does not have the same behavior as the other salts, just as the transition between low-temperature monoclinic phase to high-temperature tetragonal (instead cubic phase) must be appears at temperatures below 150ºC.[28,49,50]

CONCLUSIONS

In the present work, we have studied different compounds based CsH_2PO_4 on the partial substitution of Cs by Rb and Ba, to give $Cs_{1-x}Rb_xH_2PO_4$ and $Cs_{1-x}Ba_{0.5x}H_2PO_4$, respectively. On the other hand, the compounds named (CsP-S), (CsP-Mo), and (CsP-W). using adequate concentrations to get a 80:20 w/w, were prepared to study the conductivity, diffusion coefficient and free charge density when a morphological phase transition occurs (monoclinic to cubic phase), corresponding to a protonic and a superprotonic phase, respectively. In order to study the influence of the element dopant, the conductivity measurements have been performed as a function of the temperature in humid atmospheres. From our results an important increasing on the conductivity of the compounds is observed around 200 ºC, probably due to the disorder increment when the phase transition comes up. It is thought that the configurational entropy increase by means of Grotthuss mechanism, in which proton migration occurs via dipole reorientation, structural relaxation and proton hopping and tends to decrease the activation energy. Following the EP model from fitting data of tan δ, diffusion coefficient of protons and mobile ion concentration density have been obtained. The results show similar variations with temperature to those observed in conductivity. However, our analysis based on electrode polarization, only reflects the diffusivity of free ions, where the calculations gave a quantity of free ion concentration, *n*, lower than the total amount calculated theoretically, n_{tot}, being evident that these results have overestimated the ion diffusivity. The magnitude of these changes depends on the salt dopant, being very important in case of samples CsP, CsP-Rb and CsP-Mo. On the opposite, we observed small changes when the salt dopant used were CsS (sample, CsP-S) and BaP (CsP-Ba), respectively. The reversibility of the phase transition between low and high conductive phase has been observed around of 200ºC for all the samples except for the mixed salt CsP-S because it could have occurred at temperatures below 150ºC. The reproducibility of all the measurements has been analyzed, and that is completely satisfied. The calculated static permittivity decrease when temperature increases, and that values obtained following the Anatoli Serghei expression are smaller than obtained using the Eq. (15) obtained from the EP model.

AKNOWLEDGEMENTS

This research is support from Ministerio de Economia y Competitividad (MINECO) by mean of the project reference: ENE/2015-69203-R. ISH, CGA and SIH are grateful to project UNAM-DGAPA-PAPIIT-IN116617. SIH is grateful to project LANCAD-UNAM-DGTIC-276. LFC is grateful to projects DGAPA-PAPIIT IG-100618 and DGAPA-PAPIIT IN-114818.

REFERENCES

(1) Samms, S. R.; Wasmus, S.; Savinell, R. F.; Thermal Stability of Nafion® in Simulated Fuel Cell Environments. *J. Electrochem. Soc.* **1996**, 143, 1498-1504.

(2) Ishihara, T.; Fukui, S.; Nishiguchi, H.; Takita, Y.; Mixed Electronic-Oxide Ionic Conductor of BaCoO3 Doped with La for Cathode of Intermediate-Temperature-Operating Solid Oxide Fuel Cell. *Solid State Ionics* **2002**, 152-153, 609-613.
(3) Singh, B.; Kim, J.-H.; Parkash, O.; Song, S.-J. Effect of MnO Doping in Tetravalent Metal Pyrophosphate (MP_2O_7; M=Ce, Sn, Zr) Electrolytes. *Ceram. Int.* **2016**, 42, 2983-2989.
(4) Baranov, A.I.; Khiznichenko, V.P.; Sandler, V.A.; Shuvalov, L.A. Frequency Dielectric Dispersion in the Ferroelectric and Superionic Phases of CsH_2PO_4. *Ferroelectrics* **1988**, 81, 183-186.
(5) Baranov, A.I.; Merinov, B.V.; Tregubchenko, A.V.; Khiznichenko, V.P.; Sandler, V.A.; Shuvalov, L.A.; Schagina, N.M. Fast Proton Transport in Crystals with a Dynamically Disordered Hydrogen Bond Network. *Solid State Ionics* **1989**, 36, 279-282.
(6) Otomo, J.; Minagawa, N.; Wen, C.-J.; Eguchi, K.; Takahashi, H. Protonic Conduction of CsH_2PO_4 and its Composite with Silica in Dry and Humid Atmospheres. *Solid State Ionics* **2003**, 156, 357-369.
(7) Ortiz, E.; Vargas, R.A.; Mellander, B.-E. On the High-Temperature Phase Transitions of Some KDP-Family Compounds: A Structural Phase Transition? A Transition to a Bulk-High Proton Conducting Phase? *Solid State Ionics* **1999**, 125, 177-185.
(8) Ortiz, E.; Vargas, R.A.; Mellander, B.-E. On the High-Temperature Phase Transitions of CsH_2PO_4: A Polymorphic Transition? A Transition to a Superprotonic Conducting Phase? *J. Chem. Phys.* **1999**, 110, 4847-4853.
(9) Bronowska, W. Comment on "Does the Structural Superionic Phase Transition at 231 °C in CsH_2PO_4 Really Not Exist?" [J. Chem. Phys. **110**, 4847 (1999)]. *J. Chem. Phys.* **2001**, 114, 611-612.
(10) Klein, R.J.; Zhang, S.; Dou, S.; Jones, B.H.; Colby, R.H.; Runt, J. Modeling Electrode Polarization in Dielectric Spectroscopy: Ion Mobility and Mobile Ion Concentration of Single-Ion Polymer Electrolytes. *J. Chem. Phys.* **2006**, 124, 144903.
(11) Bandara, T.M.W.J.; Dissanayake, M.A.K.L.; Albinsson, I.; Mellander, B.-E. Mobile Charge Carrier Concentration and Mobility of a Polymer Electrolyte Containing PEO and $Pr_4N^+I^-$ Using Electrical and Dielectric Measurements. *Solid State Ionics* **2011**, 189, 63-68.
(12) Jönsson, M.; Welch, K.; Hamp, S.; Strømme, M. Bacteria Counting with Impedance Spectroscopy in a Micro Probe Station. *J. Phys. Chem. B* **2006**, 110, 10165-10169.
(13) Macdonald, J.R. Theory of ac Space-Charge Polarization Effects in Photoconductors, Semiconductors, and Electrolytes. *Phys. Rev.* **1953**, 92, 4-17.
(14) Coelho, R. Sur la Relaxation d'une Charge d'espace. *Rev. Phys. Appl.* **1983**, 18, 137-146.
(15) Sørensen, T.S.; Compañ, V. Complex Permittivity of a Conducting, Dielectric Layer Containing Arbitrary Binary Nernst-Planck Electrolytes with Applications to Polymer Films and Cellulose Acetate Membranes. *J. Chem. Soc., Faraday Trans.* **1995**, **91**, 4235-4250.
(16) Sørensen, T.S.; Compañ, V.; Diaz-Calleja, R. Complex Permittivity of a Film of Poly[4-(acryloxy)phenyl-(4-chlorophenyl)methanone] Containing Free Ion Impurities and the Separation of the Contributions From Interfacial Polarization, Maxwell–Wagner–Sillars Effects and Dielectric Relaxations of the Polymer Chains. *J. Chem. Soc., Faraday Trans.* **1996**, 92, 1947-1957.
(17) Jonscher, A.K. The 'Universal' Dielectric Response. *Nature* **1977**, 267, 673-679.
(18) Jonscher, A.K. *Dielectric Relaxation in Solids*; Chelsea Dielectric Press Limited, London, 1983.

(19) Sangoro, J.R.; Serghei, A.; Naumov, S.; Galvosas, P.; Kärger, J.; Wespe, C.; Bordusa, F.; Kremer, F. Charge Transport and Mass Transport in Imidazolium-Based Ionic Liquids. *Phys. Rev. E* **2008**, 77, 051202.
(20) Serguei, A.; Tress, M.; Sangoro, J.R.; Kremer. F. Electrode Polarization and Charge Transport at Solid Interfaces. *Phys. Rev. B* **2009**, 80, 184301.
(21) Mauritz, K.A. Dielectric Relaxation Studies of Ion Motions in Electrolyte-Containing Perfluorosulfonate Ionomers. 4. Long-Range Ion Transport. *Macromolecules* **1989**, 22, 4483-4488.
(22) Munar, A.; Andrio, A.; Iserte, R.; Compañ, V. Ionic Conductivity and Diffusion Coefficients of Lithium Salt Polymer Electrolytes Measured with Dielectric Spectroscopy. *J. Non-Cryst. Solids* **2011**, 357, 3064-3069.
(23) Wang, Y.; Sun, C.-N.; Fan, F.; Sangoro, J.R.; Berman, M.B.; Greenhaum, S.G.; Zawodzinski, T.A.; Sokolov, A.P. Examination of Methods to Determine Free-Ion Diffusivity and Number Density From Analysis of Electrode Polarization. *Phys. Rev. E* **2013**, 87, 042308.
(24) Wang, Y.; Fan, F.; Agapov, A.L.; Saito, T.; Yang, J.; Yu, X.; Hong, K.; Mays, J.; Sokolov, A.P. Examination of the Fundamental Relation Between Ionic Transport and Segmental Relaxation in Polymer Electrolytes. *Polymer* **2014**, 55, 4067-4076.
(25) Haile, S.M.; Chisholm, C.R.I.; Sasaki, K.; Boysen, D.A.; Uda, T. Solid Acid Proton Conductors: From Laboratory Curiosities to Fuel Cell Electrolytes. *Faraday Discuss.* **2007**, 134, 17-39.
(26) Leys, J.; Wübbenhorst, M.; Preethy Menon, C.; Rajesh, R.; Thoen, J.; Glorieux, C.; Nockemann, P.; Thijs, B; Binnemans, K; Longuemart, S. Temperature dependence of the electrical conductivity of imidazolium ionic liquids. *J. Chem Phys.* **2008**, 128, 064509.
(27) Greenhoe, Brian M.; Hassan, Mohammad K.; Wiggins, Jeffrey S.; Mauritz, Kenneth A. Universal power law behavior of the AC conductivity versus frequency of agglomerate morphologies in conductive carbon nanotube-reinforced epoxy networks. *J. Polym. Sci. B* **2016**, 54, 1918-1923.
(28) Haile, S.M.; Lentz, G.; Kreuer, K-D.; Maier, J. Superprotonic conductivity in $Cs_3(HSO_4)_2(H_2PO_4)$. *Solid State Ionics* **1995**, 77, 128-134.
(29) Boysen, D.; Hayle, S.M.; Liu, H.J.; Seco R.A. Conductivity of Potassium and Rubidium Dihydrogen Phosphates at High Temperature and Pressure. *Chem. Mater.* **2004**, 16, 693.
(30) Baranov, A.I.; Shuvalov, L.A.; Shchagina, N.M. Superion conductivity and phase transitions in $CsHSO_4$ and $CsHSeO_4$ crystals. *JETP Lett.* **1982**, 36, 459.
(31) Oh, S.; Insani, E.K.; Nguyen, V.H.; Kawamura, G.; Muto, H.; Sakai, M.; Matsuda, A. *Mechanochemically synthesized CsH_2PO_4–$H_3PW_{12}O_{40}$ composites as proton-conducting electrolytes for fuel cell systems in a dry atmosphere. Sci. Technol. Adv. Mater.* **2011**, 12, 034402.
(32) Komura, S.; Ohta, T. *Non-Equilibrium Soft Matter Physics (Series in Soft Condensed Matter)*; World Scientific Publishing Company; London, U.K., 2012.
(33) Louie, M.W.; Kislitsyn, M.; Bhattacharya, K.; Haile, S.M. Phase Transformation and Hysteresis Behavior in $Cs_{1-x}Rb_xH_2PO_4$. *Solid State Ionics* **2010**, 181, 173-179.
(34) Chisholm, C.R.I.; Haile, S.M. Entropy Evaluation of the Superprotonic Phase of $CsHSO_4$: Pauling's Ice Rules Adjusted for Systems Containing Disordered Hydrogen-Bonded Tetrahedra. *Chem. Mater.* **2007**, 19, 270-279.
(35) Eyring, H. The Activated Complex in Chemical Reactions. *J. Chem. Phys.* **1935**, 3, 107-115.
(36) Coelho R., On the Static Permittivity of Dipolar and Conductive Media - an Educational Approach. *J. Non-Cryst. Solids* **1991,** 131, 1136-1139.

(37) Pasini Cabello, S. D.; Mollá, S.; Ochoa, N.A.; Marchese, J., Giménez, E; V. Compañ. New Bio-polymeric Membranes Composed of Alginate-Carrageenan to be Applied as Polymer Electrolyte Membranes for DMFC. *J. Power Sources* **2014**, 265, 345-355.
(38) Altava, B.; Compañ, V.; Andrio, A.; del Castillo, L.F.; Mollá, S.; Burguete, M.I.; García-Verdugo, E.; Luis, S.V. Conductive Films Based on Composite Polymers Containing Ionic Liquids Absorbed on Crosslinked Polymeric Ionic-Like Liquids (SILLPs). *Polymer* **2015**, 72, 69-81.
(39) Fragiadakis, D.; Dou, S.; Colby, R.H.; Runt, J. Molecular mobility and Li+ conduction in polyester copolymner ionomers based on poly(ethylene oxide). *J. Chem. Phys.* **2009**, 130, 064907.
(40) Fragiadakis, D.; Dou, S.; Colby, R.H.; Runt, J. Molecular Mobility, Ion Mobility, and Mobile Ion Concentration in Poly(ethylene oxide)-Based Polyurethane Ionomers. *Macromolecules* **2008**, 41, 5723-5728.
(41) Vega, J.; Andrio A.; Lemus, A.A.; del Castillo, L.F.; Compañ, V. Conductivity Study of Zeolitic Imidazolate Frameworks, Tetrabutylammonium Hydroxide Doped with Zeolitic Imidazolate Frameworks, and Mixed Matrix Membranes of Polyetherimide/Tetrabutylammonium Hydroxide Doped with Zeolitic Imidazolate Frameworks for Proton Conducting Applications. *Electrochim. Acta* **2017**, 258, 153-166.
(42) Garcia-Bernabé, A.; Compañ, V.; Burguete, M.I.; García-Verdugo E.; Karbass, N; Luis S.V.; Riande, E. Conductivity and Polarization Processes in Highly Cross-Linked Supported Ionic Liquid-Like Phases. *J. Phys. Chem. C* **2010**, 114, 7030-7037.
(43) Colomban, P.; Badot, J.C. Radiowave and Microwave Frequency Dielectric Relaxations at the Superionic, Incommensurate and Ferroelectric Phase Transitions in NH_4HSeO_4 and ND_4DSeO_4. *J. Phys.: Condens. Matter* **1992**, 4, 5625-5638.
(44) Híjar, H.; Méndez-Bermúdez, J. G.; Santamaría-Holek, Iván, Mesoscopic nonequilibrium thermodynamics approach to non-Debye dielectric relaxation. *J. Chem. Phys.* **2010**, 132, 084502.
(45) Wübbenhorst, M.; van Turnhout, J. Analysis of Complex Dielectric Spectra. I. One-Dimensional Derivative Techniques and Three-Dimensional Modelling. *J. Non-Cryst. Solids* **2002**, 305, 40-49.
(46) Choi, U.H.; Mittal, A.; Price Jr, T.L.; Gibson, H.W.; Runt, J.; Colby, R.H. Polymerized Ionic Liquids with Enhanced Static Dielectric Constants. *Macromolecules* **2013**, 46, 1175-1186.
(47) Lee, H.-S.; Tuckerman, M.E. The Structure and Proton Transport Mechanisms in the Superprotonic Phase of CsH_2PO_4: An Ab Initio Molecular Dynamics Study. *J. Phys. Chem. C* **2008**, 112, 9917-9930.
(48) Garcia Bernabe, A.; Rivera-Sancho, A.: Granados, A.; Luis, S.V.: Compañ Moreno, V. Ionic transport on composite polymers containing covalently attached and absorbed ionic liquid fragments. Electrochimica Acta. **2016**, 213, 887-897.
(49) Ponomareva, V. G.; Bagryantseva, I. N.; Lavrova, G. V.; Moroz, N. K. Investigation of $Cs(H2PO4)_{1-x}(HSO4)_x$ (x = 0.15–0.3) Superprotonic Phase Stability. Inorg. Mater. **2014**, 50, 716-722.
(50) Ponomareva, V. G.; Bagryantseva, I.N. Superprotonic CsH_2PO_4-$CsHSO_4$ Solid Solutions. Inorganic Materials , **2008**, 48, 187-194.